

# Adaptive nonreciprocal wave attenuation in linear piezoelectric metastructures shunted with one-way electrical transmission lines

Yisheng Zheng, Yegao Qu\*, Guang Meng

State Key Laboratory of Mechanical System and Vibration, Shanghai Jiao Tong University, 200240, Shanghai, China

\*Corresponding author, Email: quyegao@sjtu.edu.cn (Y. Qu).

In contrary to elastic mediums, it is easy to attain one-way coupling feature among electrical elements, which enables the achievement of unidirectional electrical energy transmission. In this letter, we explore and exploit the interaction of one-way electrical transmission lines with piezoelectric beams to facilitate nonreciprocal transmission of elastic wave in the linear fashion. Theoretical dispersion analysis and numerical simulations are performed to reveal transmission behaviors of elastic wave in the presented piezoelectric metastructure. It is uncovered that the local-resonance bandgaps of the piezoelectric metastructure are maintained for both directions when the one-way electrical coupling feature is introduced. However, the wave attenuation capability in the bandgap is distinct for the two opposite directions, which thus enables nonreciprocity of elastic wave. It is also revealed that the nonreciprocal wave attenuation capability is adaptive with the one-way electrical coupling coefficient. Overall, the presented piezoelectric metastructure provides a linear and concise means to realize adaptive nonreciprocity of elastic wave.

In regular elastic mediums, the transmission of elastic/acoustic wave obeys the reciprocity theorem<sup>1</sup>. There have been many efforts trying to break this limitation to achieve unidirectional elastic/acoustic transmission, among which the scheme utilizing nonlinear properties of elastic mediums is the first one proposed<sup>2</sup>. It may also be the most common one investigated to date and all sorts of nonlinear nonreciprocal systems have been explored<sup>3-7</sup>. However, the approach utilizing nonlinearity usually would disturb the energy frequency, which is an important characteristic needed to be reserved during wave propagation process, especially if the wave is regarded as signals rather than just energy. Besides, the nonlinear approaches have strict restrictions on excitation amplitudes that induce nonreciprocity. Therefore, it is significantly vital to explore linear elastic systems to achieve nonreciprocity. Fleury et al.<sup>8</sup> performed a pioneer work to investigate a linear acoustic circulator with nonreciprocity. The spatial-temporal modulation is also known as an effective linear means to achieve nonreciprocal elastic wave<sup>9,10</sup>. Though several experimental works have been reported<sup>11-13</sup>, the physical implementation of this sort of nonreciprocal system is still complicated since special control techniques are required to modulate its physical parameters such as modulus and density in both the space and time domain. In recent years, the linear approaches utilizing active control are also studied to facilitate nonreciprocity, including the acoustic duct using eigen-structure assignment control strategy<sup>14</sup>, the non-local active acoustic

metamaterials<sup>15</sup> and the active mechanical Willis meta-layer<sup>16</sup>. Generally, it is still challenging to design concise nonreciprocal elastic/acoustic systems in the linear fashion.

Actually, we can achieve nonreciprocity readily if one-way physical couplings are attainable. Figure 1. (a) shows the schematic of a one-way coupling physical system, where neighboring two mediums are coupled in the on-way fashion, viz. the response of medium  $j$  ( $j=1, 2 \dots N-1$ ) can affect that of medium  $j+1$  but not the reverse. In such a system, the physical wave can propagate from medium 1 to medium  $N$  unidirectionally. However, based on the Newton's third law, which states that the reaction force equals to the action force, it is nearly impossible to attain the one-way coupling feature in conventional elastic mediums and thus it is difficult to achieve nonreciprocal elastic wave. On the contrary, it is much easier to attain the one-way coupling feature in electrical systems, such as that the commonly used dependent sources can work as one-way coupling elements. We present one such one-way coupling electrical element in Fig. 1(b), which can be seen as a voltage-controlled voltage source (VCVS). The response  $U_o$  depends on  $U_i$  while  $U_i$  is not affected by the VCVS and electrical elements connected with its output node. It is worth noting that the electrical diode is also a nonreciprocal device but only used to attain nonreciprocity for DC signals. Utilizing one-way coupling electrical elements, the one-way electrical transmission line that allows nonreciprocal electrical wave could be

conveniently established. This sort of one-way coupling feature undertakes similarity with the active control strategy where control signals transmit unidirectionally, which has been used to attain acoustic nonreciprocity<sup>14,15</sup>.

In this research, driven by the idea of “what happens if a two-way elastic medium is coupled with a one-way electrical transmission line”, we explore elastic wave transmission behaviors in a linear piezoelectric metastructure as shown in Fig. 2. It constitutes of a piezoelectric beam with periodically distributed PZT patches and a shunted one-way electrical transmission line. Actually, the approach of coupling elastic systems with electrical systems utilizing piezoelectric effects has proved great effectiveness and adaptiveness in manipulating elastic wave propagation for functionalities such as bandgap<sup>17,18</sup>, beam steering<sup>19</sup>, wave filtering<sup>20</sup>, topological insulation<sup>21</sup> and nonreciprocity<sup>16,22</sup>. Especially, piezo-metamaterials employing two-way electrical transmission lines have also been studied for elastic wave and vibration control<sup>23,24</sup>. Distinguished from these works, the shunting circuits in the presented metastructure is a one-way electrical transmission line. We uncover that the behavior of adaptive nonreciprocal wave attenuation exits in such an electrical-mechanical system.

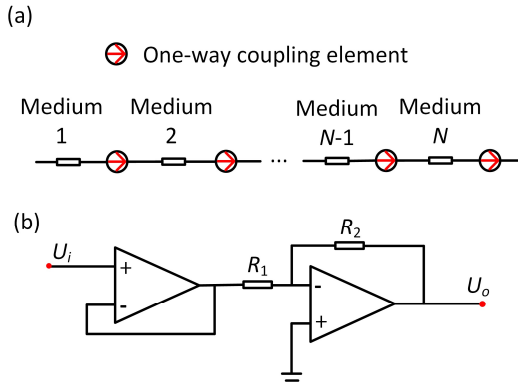
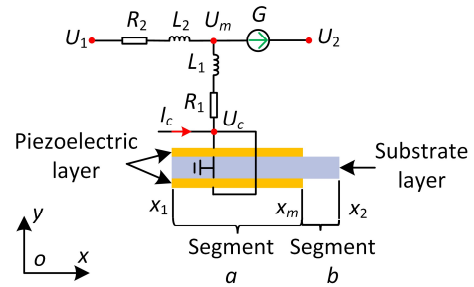


Fig. 1 (a) Schematic of physical systems with unidirectional wave transmission, neighboring mediums are coupled in the one-way fashion. (b) Diagram of one-way coupling electrical elements consisting of a voltage buffer and an inverting amplifier; the coupling coefficient  $G = -R_2 / R_1$ , which relates the input voltage  $U_i$  and the output voltage  $U_o$  as  $U_o = G \cdot U_i$ .

The electrical-mechanical unit cell of the metastructure is illustrated in Fig. 2 (a). Two PZT patches are bonded to opposite sides of the substrate layer, which are connected in the parallel configuration. For the electrical transmission line, neighboring cells are coupled in the one-way fashion by using one-way coupling electrical elements presented as Fig.

1(b). The voltage  $U_m$  and  $U_2$  is governed by the relation  $U_2 = G \cdot U_m$  and the input current to the one-way coupling electrical element is 0. It is readily recognized that elastic wave propagation in the piezoelectric beam alone is reciprocal while electric wave in the electrical transmission line alone is nonreciprocal. However, due to the interaction between the piezoelectric beam and electrical transmission line, wave transmission properties in the coupled electrical-mechanical system deserves further exploration. We would investigate wave transmission properties in both directions of the system so as to reveal its nonreciprocity.

(a) One-way coupling electrical element



(b)

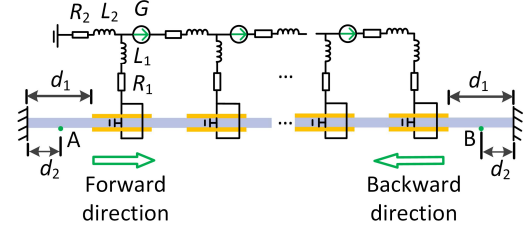


Fig. 2 (a) Unit-cell of piezoelectric metastructure, the diagram of one-way coupling electrical element is given as Fig. 1(b),  $I_c$  is the current generated by PZT patches. (b) Nonreciprocal piezoelectric metastructures shunted with a one-way electrical transmission line: for forward transmission, the force  $F$  is applied at point A and the acceleration  $a_s$  of point B is measured; for backward transmission, the force  $F$  is applied at point B and the acceleration  $a_s$  of point A is measured.

For the purpose of modelling and calculation, parameters of the metastructure cell are first illustrated in the following. The length of cells is  $l_c = 17$  mm. The cross-section size of the substrate layer is  $b \times h = 15 \times 2$  mm. The length and cross-section size of PZT patches are  $l_p = 15$  mm and  $b_p \times h_p = 15 \times 1$  mm, respectively. The density and Young's modulus of the Aluminum beam are respectively  $E = 69$  GPa and  $\rho = 2700$  Kg/m<sup>3</sup> while that of PZT patches are respectively  $E_p = 60$  GPa and  $\rho = 7780$  Kg/m<sup>3</sup>. The piezoelectric strain constant is  $d_{31} = -1.7 \times 10^{-10}$  C/N. The dielectric

constant is  $\epsilon_{33}^T = 1.6 \times 10^{-8}$  F/m. For each cell, the capacitance of PZT patches at constant strain is calculated as  $C_p = 6.4$  nF. Parameters of the electrical transmission line are as given follows:  $L_1 = 0.1$  H,  $L_2 = 0.1$  H,  $R_1 = 100 \Omega$  and  $R_2 = 100 \Omega$ .

To analyze nonreciprocity of the proposed electrical-mechanical system, we deduce its dispersion relation using the transfer matrix method<sup>25</sup>. Considering the Euler beam assumption, the dynamic variables of the beam is given as  $\mathbf{Y} = [w \ w_x \ M \ Q]^T$ .  $w$  and  $w_x$  are the transverse displacement and its derivative with respect to the position  $x$ , respectively;  $M$  and  $Q$  are the bending torque and shear force, respectively. For the beam segment  $a$  with PZT layers, as shown in Fig. 2(a), the dynamic equations in frequency domain is presented as

$$\begin{cases} \frac{dw}{dx} = w_x, D_a \frac{dw_x}{dx} = M + \mu U_c \\ \frac{dM}{dx} = -Q, \frac{dQ}{dx} = -\omega^2 m_a w \end{cases} \quad (1)$$

where  $D_a$  and  $m_a$  are the bending rigidity and linear mass density of segment  $a$ , respectively.  $U_c$  is the voltage on PZT patches. The electrical-mechanical coupling coefficient  $\mu$  is given as<sup>26</sup>

$\mu = E_p d_{31} b_p \cdot (h_p + h_b)$ . Eq. (1) can be rearranged into the matrix form as

$$\mathbf{Y}' = \mathbf{C}_a \cdot \mathbf{Y} + \mathbf{J}_a \cdot U_c \quad (2)$$

with

$$\mathbf{C}_a = \begin{bmatrix} 0 & 1 & 0 & 0 \\ 0 & 0 & 1/D_a & 0 \\ 0 & 0 & 0 & -1 \\ -\omega^2 m_a & 0 & 0 & 0 \end{bmatrix}, \mathbf{J}_a = \begin{bmatrix} 0 \\ \mu/D_a \\ 0 \\ 0 \end{bmatrix} \quad (3)$$

As for Eq. (2), letting  $U_c = 0$  and replacing  $\mathbf{C}_a$  with  $\mathbf{C}_b$ , we can obtain the similar formulation for segment  $b$ .  $\mathbf{C}_b$  is achieved by simply replacing  $D_a$  and  $m_a$  in Eq. (3) with  $D_b$  and  $m_b$ , respectively. From Eq. (2), we can derive the relation between  $\mathbf{Y}$  at position  $x_1$  and that at position  $x_2$ , given as

$$\mathbf{Y}_2 = \mathbf{H} \cdot \mathbf{F} \cdot \mathbf{Y}_1 + \mathbf{B} \cdot U_c \quad (4)$$

where  $\mathbf{F} = e^{\mathbf{C}_a \cdot l_p}$ ,  $\mathbf{H} = e^{\mathbf{C}_b \cdot (l_c - l_p)}$  and the coupling matrix  $\mathbf{B}$  is written as  $\mathbf{B} = (\mathbf{H} \cdot \mathbf{F} - \mathbf{H}) \cdot \mathbf{C}_a^{-1} \cdot \mathbf{J}_a$ .

For the electrical cell shown in Fig. 2(a), the following dynamic equations can be formulated

$$U_c = (1 + Z_1/Z_2)/G \cdot U_2 - Z_1/Z_2 \cdot U_1 \quad (5)$$

$$(Z_1 + Z_2 + Z_c)/G \cdot U_2 = (Z_1 + Z_c)U_1 + Z_c Z_2 I_c \quad (6)$$

where  $Z_1 = L_1 s + R_1$ ,  $Z_2 = L_2 s + R_2$ ,  $Z_c = 1/(C_p s)$ . Eq. (5) can be substituted into Eq. (4) for eliminating the variable  $U_c$ . For Eq. (6), the current  $I_c$  generated by PZT patches in each cell

is  $I_c = -s \mu \mathbf{J}_b \cdot (\mathbf{Y}_m - \mathbf{Y}_1)$ , where  $s$  is the complex number,  $\mathbf{J}_b = [0 \ 1 \ 0 \ 0]$  and  $\mathbf{Y}_m = \mathbf{H}^{-1} \cdot \mathbf{Y}_2$ . We can then combine Eqs. (4) and (6) to formulate the following equation

$$\mathbf{X}_2 = \mathbf{T}_c \cdot \mathbf{X}_1 \quad (7)$$

with  $\mathbf{X}_i = [\mathbf{Y}_i \ U_i]^T$ ,  $i = 1, 2$  and  $\mathbf{T}_c = \mathbf{P}^{-1} \cdot \mathbf{Q}$ . The terms  $\mathbf{P}$  and  $\mathbf{Q}$  are given as

$$\begin{cases} \mathbf{P} = \begin{bmatrix} \mathbf{I}_{4 \times 4} & -(1 + Z_1/Z_2)/G \cdot \mathbf{B} \\ s \mu Z_c Z_2 \cdot \mathbf{J}_b \cdot \mathbf{H}^{-1} & (Z_1 + Z_2 + Z_c)/G \end{bmatrix} \\ \mathbf{Q} = \begin{bmatrix} \mathbf{H} \cdot \mathbf{F} & -Z_1/Z_2 \cdot \mathbf{B} \\ s \mu Z_c Z_2 \cdot \mathbf{J}_b & Z_1 + Z_c \end{bmatrix} \end{cases} \quad (8)$$

According to the Floquet-Bloch theorem, the relation between  $\mathbf{X}_1$  and  $\mathbf{X}_2$  could also be written as

$$\mathbf{X}_2 = e^{jk \cdot l_c} \mathbf{X}_1 \quad (9)$$

where  $k$  is the wavenumber and  $j$  is the imaginary unit. From Eqs. (7) and (9), the dispersion relation of the electrical-mechanical system can be presented as

$$|\mathbf{T}_c - e^{jk \cdot l_c} \mathbf{I}| = 0 \quad (10)$$

For a given frequency  $\omega$ , the calculated  $k$  could be expressed in the complex form. The imaginary part of wavenumber  $k$  determines the wave attenuation constant  $\mu$  of the metastructure based on the expression  $\mu = \text{imag}(k) \cdot l_c$ . Therefore, the value  $\text{imag}(k)$  can reflect the wave attenuation capability of the system.

With Eq. (10), we can then calculate the dispersion diagrams of the electrical-mechanical metastructure, which are presented as Fig. 3. We firstly consider the scenario when  $G$  is extremely small,  $G = -0.001$  is chosen herein, the results of which are given in Fig. 3(a). As depicted in Fig. 3(a.1), one branch represents dispersion of the electrical transmission line and the other four branches represent two propagating elastic wave modes and two evanescent elastic wave modes of the beam. Since  $\text{imag}(k)$  indicates wave attenuation capability, we can know from Fig. 3(a.2) that the electrical wave attenuation is very large and its transmission can be ignored. Also, figure 3(a.3) shows that  $\text{imag}(k)$  is almost the same for the two propagating elastic wave modes and appears to be large around the circuit natural frequency  $f_n = 1/(2\pi \sqrt{(L_1 + L_2) \cdot C_p}) = 4450$  Hz, which indicates that local-resonance bandgaps exist in the system and the wave attenuation capability in the bandgap are the same for both directions. These phenomena can be attributed to the extremely small coupling effect between

neighboring electrical cells, which leads to little electrical energy transmission through the electrical system. Thus, the electrical circuits and the mechanical structure are locally interacted and all electrical cells work as shunting local resonators for the piezoelectric beam. Actually, when  $G$  equals to 0, we can readily know from Fig. 2(b) that the electrical-mechanical system degenerates into a conventional local-resonance piezoelectric metastructure shunted with inductors ( $L=L_1+L_2$ ) in series with resistors ( $R=R_1+R_2$ ). It is understood that reciprocal local-resonance bandgaps exist in such systems. Therefore, the results of the case  $G=-0.001$  corroborate with the known properties of local-resonance piezoelectric metastructures. When the one-way coupling coefficient  $G$  is increased to be  $G=-0.05$ , as depicted in Figs. 3(b.2), the dispersion branch of the electrical transmission line approaches the horizontal axis, which indicates that the transmission capability of energy in the electrical transmission line is improved obviously and thus cannot be ignored. From the zoom-in view of dispersion curves

presented in Fig. 3(b.3), it is interesting to find that the  $\text{imag}(k)$  is still large around circuit natural frequency  $f_n$ . Thus, the bandgap based on the local-resonance mechanism is maintained even with the existence of wave propagation in the electrical transmission line. It is distinct from piezoelectric metamaterials with two-way shunting electrical transmission lines where the bandgap is characterized by dispersion veering and crossing effects<sup>24,27,28</sup>. Due to the significant interaction between transmission of electrical energy and that of mechanical energy, the obvious shape alteration of  $\text{imag}(k)$  curves for the propagating elastic waves and the electrical wave is also observed around the bandgap. As depicted in Fig. 3(b.3), the  $\text{imag}(k)$  curves are not symmetric about the horizontal axis anymore, which implies appearance of nonreciprocal wave attenuation in this scenario. Its underlying mechanism is that the transmission of energy in the electrical transmission line is unidirectional, which thus manipulates the transmission of mechanical energy direction-dependently.

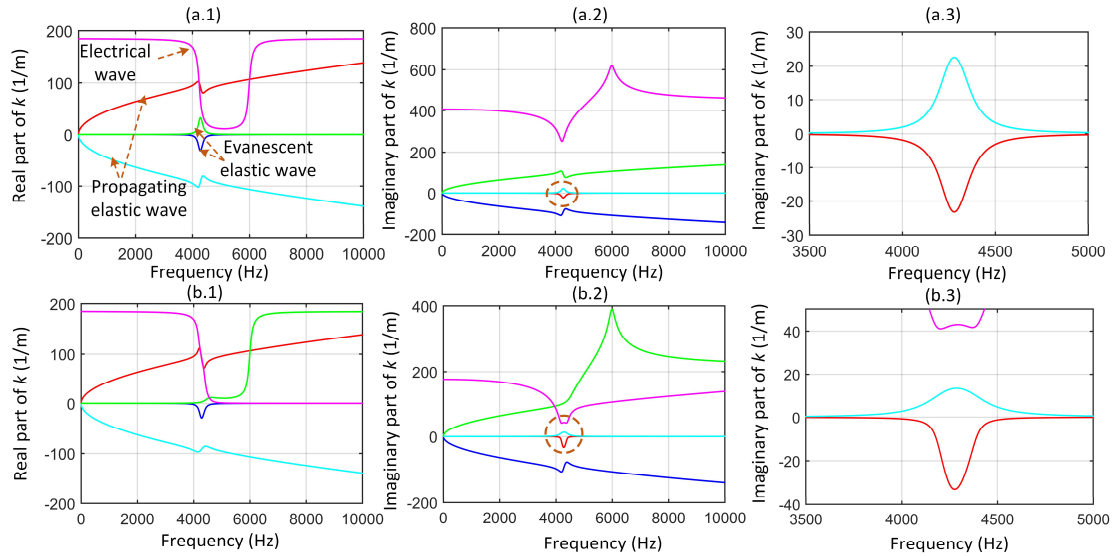


Fig. 3 Dispersion relations of the piezoelectric metastructure with different one-way electrical coupling coefficients  $G$ : (a)  $G=-0.001$ ; (b)  $G=-0.05$ . Figures (a.1) and (b.1) present the real part of wave number  $k$  while Figs. (a.2) and (b.2) present the corresponding imaginary parts of wavenumber  $k$  using the same color lines. Figures (a.3) and (b.3) present the zoom-in views of the dashed-circle areas in Figs. (a.2) and (b.2), respectively.

To illustrate nonreciprocity more intuitively and characterize its intensity quantitatively, we further utilize the FEM software Comsol Multiphysics to investigate wave transmission properties in the finite piezoelectric metastructure shown in Fig. 2(b). The piezoelectric beam is fixed on both ends. The electrical transmission line is grounded on the left end while the right end is open. The piezoelectric metastructure has 16 cells, which is located at the position  $d_1=275$  mm

from the ends of the beam. The total length of the beam is  $d=820$  mm. The two points A and B are designated for actuating and sensing and they are positioned at  $d_2=100$  mm from the ends of the beam. We employ the voltage-controlled voltage source in the Electrical-circuit physics to model the one-way coupling electrical element presented as Fig. 1(b). For the Comsol-based FE model, the Rayleigh damping is applied to the mechanical structures and a weak damping ratio

$\zeta = 10^{-4}$  is assumed. When examining the forward wave propagation behaviors, the harmonic force  $F$  is applied at point A and the acceleration  $a_s$  of point B is measured. On the contrary, when the backward wave propagation behaviors are considered, the force  $F$  is applied at point B and the acceleration  $a_s$  of point A is measured. The frequency response function (FRF)  $a_s/F$  is defined to evaluate wave transmission.

For the presented metastructure with different circuit conditions, the calculated frequency response functions  $a_o/F$  are depicted in Fig. 4(a). It is seen that when the electrical transmission line is disconnected with PZT patches, namely “open circuit” case, there exists no local-resonance bandgaps. This case is used as the comparing reference to indicate wave attenuation properties induced by the shunted electrical transmission line. When the electrical transmission line is shunted and its one-way coupling coefficient  $G=0$ , the local-resonance bandgap is clearly observed around the circuit natural frequency  $f_n$ . It is known from Fig. 3 that when the one-way coupling coefficient  $G$  is nonzero, the forward and backward wave attenuation capability would be altered. Here we calculate frequency response functions  $a_s/F$  under different nonzero  $G$ . The

results in Fig. 4(a) indicate that for the cases with  $G=-0.05$ ,  $-0.10$  and  $-0.15$ , the wave attenuation around  $f_n$  exists for the two opposite directions, viz. the local-resonance bandgaps are maintained when the one-way electrical coupling feature is introduced. Additionally, it is seen that the backward attenuation capability is improved compared with the “local-resonance” case while that in forward direction is weakened. Therefore, the wave attenuation capability of the opposite directions is distinguished and nonreciprocity emerges. Lastly, we find that if the one-way coupling coefficient  $G$  is increased, the forward transmission in the bandgap is increased while the backward transmission is decreased. This feature enlightens us that the asymmetry ratio of the presented nonreciprocal metastructure can be changed by adjusting  $G$ . Fig. 4(b) further presents the acceleration distribution of the piezoelectric metastructure at frequency  $f=4290$  Hz within the bandgap. It is seen that, for all cases, elastic wave decays more drastically in the backward direction, which implies larger wave attenuation capability. Moreover, if  $G$  is increased, the backward transmitted elastic energy tends to be localized around the input end. These numerical results could well verify nonreciprocity of the presented system and its adaptiveness.

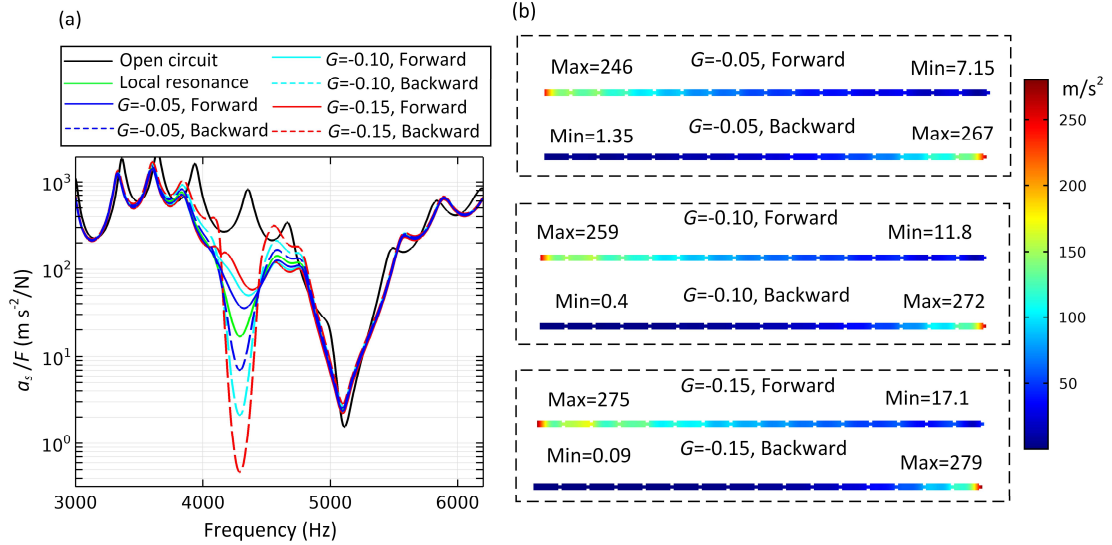


Fig. 4 (a) Numerical frequency response functions (FRFs)  $a_s/F$  of the piezoelectric metastructure: for the case “open circuit”, the electrical transmission line is disconnected with PZT patches; for the case “local resonance”, the one-way electrical coupling coefficient  $G$  equals to 0 and the system becomes a conventional local-resonance piezoelectric metamaterial; for cases with different nonzero  $G$ , FRFs in both directions are calculated to reveal nonreciprocity. (b) Acceleration distribution along the piezoelectric metastructure with excitation frequency fixed in the bandgap,  $f=4290$  Hz chosen herein, where the maximum and minimum values of acceleration amplitude are also illustrated.

We further calculate time-domain acceleration responses of the piezoelectric metastructure using the Comsol multiphysics. Three scenarios with different  $G$  are considered:  $G=-0.05$ ,  $G=-0.10$ ,  $G=-0.15$ . The actuating and sensing conditions are the same with that in the frequency-domain

analysis. The excitation frequency  $f=4290$  Hz in the bandgap is chosen. The steady response in an interval of  $\Delta t=0.01$ s is recorded and present in Fig. 5. It verifies the existence of nonreciprocity in the proposed system. Also, the nonreciprocity can be enhanced by enlarging the one-way



electrical coupling coefficient  $G$ . The time-domain results corroborate with conclusions obtained in the frequency-domain analysis. In the time-domain analysis, it is also observed that the electrical-mechanical system becomes unstable if the one-way coupling coefficient  $G$  exceeds certain critical values, which is common in systems with active elements<sup>13,15,16</sup>. Thus, though increasing the coupling coefficient  $G$  could lead to stronger nonreciprocity, we need to limit  $G$  in the designing process to guarantee stability of the system.

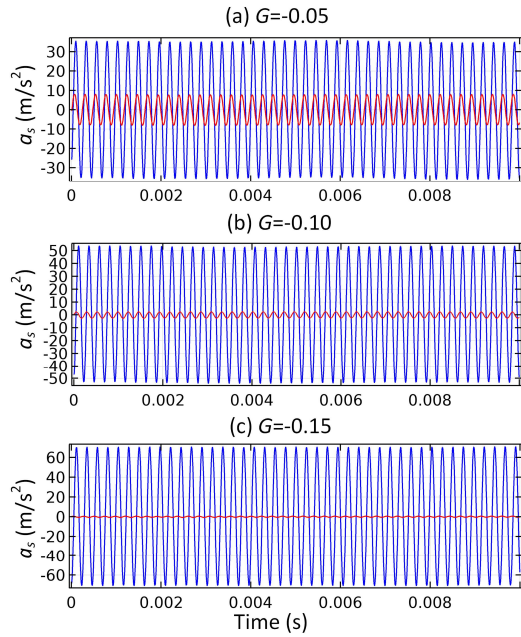


Fig. 5 Numerical time-domain acceleration responses indicating forward transmission (blue, sensing point B) and backward transmission (red, sensing point A) of elastic wave, the excitation frequency is at 4290 Hz of the bandgap.

In conclusion, we have reported a linear and concise scheme to attain nonreciprocal elastic wave transmission, which relies on the interaction between reciprocal piezoelectric beams and nonreciprocal electrical transmission lines. Equipped with a one-way electrical transmission line shunting, the presented electrical-mechanical system is found to maintain the local-resonance bandgap in both directions but with distinguished wave attenuation capability, which therefore leads to nonreciprocity. This phenomenon is fundamentally distinct from that in piezoelectric metamaterials shunted with two-way electrical transmission lines. Furthermore, the asymmetry ratio of the presented nonreciprocal system is adaptive with the one-way electrical coupling coefficient. Though nonreciprocity mechanism in this letter is based on local-resonance bandgaps, we expect that it is also attainable in the broadband Bragg-type bandgaps, which remains to be studied in the future. Additionally, the one-

way electrical coupling feature could also be introduced to manipulate elastic wave in 2D electrical-mechanical systems. Lastly, we envision that the concept of employing nonreciprocity of electrical wave to induce nonreciprocity of elastic wave could possibly be extended to explore interactions of other nonreciprocal physical mediums with elastic mediums.

This research was funded by the National Natural Science Foundation of China (No. 12002203) and the China Postdoctoral Science Foundation (No. 2020M671105).

#### DATA AVAILABILITY

The data that support the findings of this study are available from the corresponding author upon reasonable request.

#### REFERENCES

- <sup>1</sup> J.W. Strutt, Proc. London Math. Soc. **s1-4**, 357 (1871).
- <sup>2</sup> B. Liang, B. Yuan, and J.C. Cheng, Phys. Rev. Lett. **103**, 104301 (2009).
- <sup>3</sup> N. Boechler, G. Theocharis, and C. Daraio, Nat. Mater. **10**, 665 (2011).
- <sup>4</sup> S. Lepri and G. Casati, Phys. Rev. Lett. **106**, 164101 (2011).
- <sup>5</sup> B.I. Popa and S.A. Cummer, Nat. Commun. **5**, 3398 (2014).
- <sup>6</sup> Z. Wu, Y. Zheng, and K.W. Wang, Phys. Rev. E **97**, 022209 (2018).
- <sup>7</sup> Y. Zheng, Z. Wu, X. Zhang, and K.W. Wang, Smart Mater. Struct. **28**, 045005 (2019).
- <sup>8</sup> R. Fleury, D.L. Sounas, C.F. Sieck, M.R. Haberman, and A. Alù, Science (80-. ). **343**, 516 (2014).
- <sup>9</sup> G. Trainiti and M. Ruzzene, New J. Phys. **18**, 083047 (2016).
- <sup>10</sup> H. Nassar, X.C. Xu, A.N. Norris, and G.L. Huang, J. Mech. Phys. Solids **101**, 10 (2017).
- <sup>11</sup> Y. Wang, B. Yousefzadeh, H. Chen, H. Nassar, G. Huang, and C. Daraio, Phys. Rev. Lett. **121**, 194301 (2018).
- <sup>12</sup> Y. Chen, X. Li, H. Nassar, A.N. Norris, C. Daraio, and G. Huang, Phys. Rev. Appl. **11**, 064052 (2019).
- <sup>13</sup> J. Marconi, E. Riva, M. Di Ronco, G. Cazzulani, F. Braghin, and M. Ruzzene, Phys. Rev. Appl. **13**, 031001 (2020).
- <sup>14</sup> A. Baz, J. Acoust. Soc. Am. **147**, 2656 (2020).
- <sup>15</sup> A. Sasmal, N. Geib, B.I. Popa, K. Grosh, and K. Grosh, New J. Phys. **22**, 063010 (2020).
- <sup>16</sup> Y. Chen, X. Li, G. Hu, M.R. Haberman, and G. Huang, Nat. Commun. **11**, 3681 (2020).
- <sup>17</sup> O. Thorp, M. Ruzzene, and A. Baz, Smart Mater. Struct. **10**, 979 (2001).
- <sup>18</sup> C. Sugino, M. Ruzzene, and A. Erturk, Phys. Rev. Appl. **13**, 061001 (2020).
- <sup>19</sup> J. Xu and J. Tang, Appl. Phys. Lett. **110**,

181902 (2017).

<sup>20</sup> G. Trainiti, Y. Xia, J. Marconi, G. Cazzulani, A. Erturk, and M. Ruzzene, Phys. Rev. Lett. **122**, 124301 (2019).

<sup>21</sup> A. Darabi, M. Collet, and M.J. Leamy, Proc. Natl. Acad. Sci. **117**, 16138 (2020).

<sup>22</sup> C. Sugino, M. Ruzzene, and A. Erturk, Phys. Rev. B **102**, 014304 (2020).

<sup>23</sup> B. Lossouarn, M. Aucejo, and J.-F. Deü, Smart Mater. Struct. **24**, 045018 (2015).

<sup>24</sup> E.A. Flores Parra, A. Bergamini, B. Van Damme, and P. Ermanni, Appl. Phys. Lett. **110**,

184103 (2017).

<sup>25</sup> L. Airolidi and M. Ruzzene, New J. Phys. **13**, 113010 (2011).

<sup>26</sup> C. Sugino, S. Leadenham, M. Ruzzene, and A. Erturk, Smart Mater. Struct. **26**, 055029 (2017).

<sup>27</sup> E.A.F. Parra, A. Bergamini, L. Kamm, P. Zbinden, and P. Ermanni, Smart Mater. Struct. **26**, 067001 (2017).

<sup>28</sup> A.E. Bergamini, M. Zündel, E.A. Flores Parra, T. Delpero, M. Ruzzene, and P. Ermanni, J. Appl. Phys. **118**, 154310 (2015).